Mesoscale Boundary-Layer Evolution over Complex Terrain. Part II: Factors Controlling Nocturnal Boundary-Layer Structure

DAVID C. BADER

Pacific Northwest Laboratory, Richland, Washington

THOMAS B. MCKEE

Department of Atmospheric Science, Colorado State University, Fort Collins, Colorado

(Manuscript received 15 January 1991, in final form 27 August 1991)

ABSTRACT

The development of the nocturnal boundary layer (NBL) over a sloping plateau upwind of a high mountain barrier is studied with a numerical model and field observations. Six numerical simulations and one observed case are used to describe the effects of wind speed, wind direction, and sunset mixed-layer depth on the NBL structure 6 h after sunset. When there is a component of wind into barrier, a two-layer structure develops. A 75–175-m-deep inversion layer that is topped by a 200–300-m-deep, less stable transition layer extends over the length of the plateau. Shear between the 3–4 m s^{-1} drainage winds in the inversion layer and the large-scale wind mix cold air vertically to build the transition layer. The inversion layer appears to be relatively insensitive to changes in the external parameters, but transition-layer depth is proportional to wind speed.

1. Introduction

The nocturnal boundary-layer evolution over mountainous terrain is difficult to study observationally because the interaction of landforms with the atmosphere typically produces a complicated layered structure. In an earlier paper (Bader et al. 1987), hereinafter referred to as Part I, the diurnal evolution of a meso-β-scale boundary layer was studied using a combination of observational data and numerical model results. Figure 1 shows a map of the primary study area known as the Roan Plateau, a broad sloping plateau between the Colorado and White rivers in northwestern Colorado. The principal result of Part I was a description of how a deep, weakly stable nocturnal boundary layer (NBL) developed above the plateau, which lies on the upwind side of a high mountain barrier. The shear between the topographically induced nocturnal flows and the overlying synoptic winds mixed the cold air near the surface upward to build a 500–800-m-deep isothermal layer by sunrise. Local slope and valley flows were buffered from the large-scale wind field by this deep NBL until it was destroyed by convective circulations several hours after sunrise.

We continue to study the structure and evolution of the mesoscale NBL in the present paper through an examination of the factors that contribute to its day-to-day and seasonal variability. The prime motivation for this study is the observed persistence of local valley and slope flows in the valleys that cut into the plateau, despite the wide variability observed in the synoptic-scale meteorology. During the day, surface heating produces convective motions that couple the valley atmosphere and the overlying synoptic wind. In the past, it was thought that the mechanical effects of topographic sheltering were the dominant effects that decoupled the slope and valley circulations from the overlying winds once the daytime heating was replaced by nocturnal cooling. As was seen in Part I, however, the thermal stability of the NBL that extends over the ridgetop plateau inhibits turbulent mixing between the synoptic flow and underlying valley and slope winds. The plateau circulation results from the nonlinear, time-dependent interaction between the mechanical and thermal effects produced by complex terrain landforms. This circulation does not conform to the assumptions used in either linear potential flow theory or steady-state boundary-layer turbulence models.

As before, the primary tool for this study was a modified version of the multidimensional, nonhydrostatic, cloud and mesoscale model developed by Tripoli and Cotton (1982, 1986). The numerical model was not used for detailed studies of specific observed cases, but instead was used in a series of idealized experiments designed to isolate the dominant influences of the high plateau on boundary-layer structure. In this respect, the numerical model fills a role similar to that of physical models, such as wind tunnels and towing tanks.

Corresponding author address: Dr. David C. Bader, Battelle Northwest Labs, 901 D St. SW, Suite 900, Washington, DC 20024-2115.

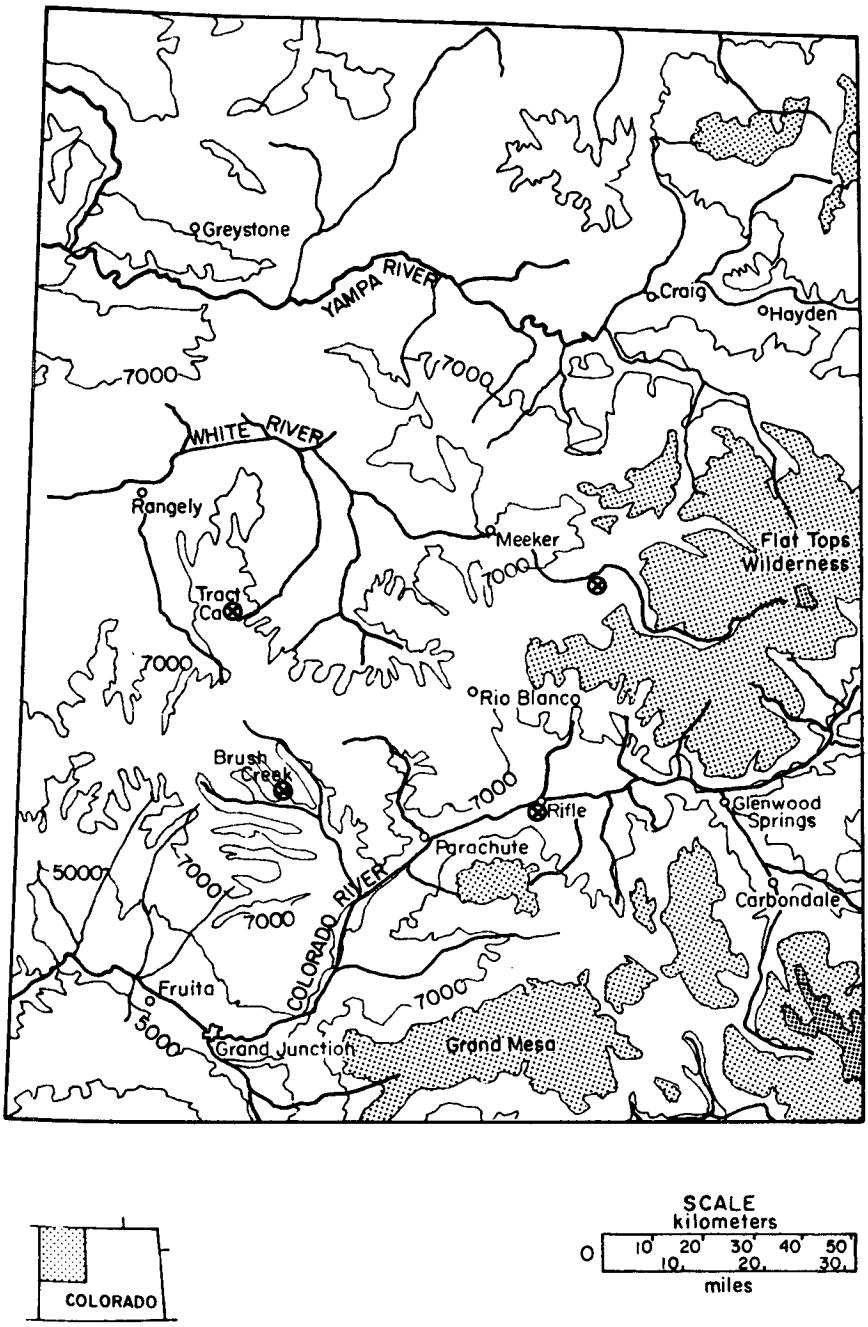

FIG. 1. Map of northwest Colorado showing the Roan Plateau. Contour intervals are 2000 ft, and area with elevations above 9000 ft are shaded.

The numerical model has the advantage of being able to simulate the atmospheric processes on the scale of interest, in this case a 50-km-wide boundary layer on the upwind side of a high mountain barrier. However, the numerical results must be examined carefully to ensure that the model assumptions, formulation, and boundary conditions reproduce physically realistic solutions.

Results from model simulations and one observed case of NBL development are presented that demonstrate the effects of wind speed, wind direction, and initial daytime mixed-layer depth on the nocturnal wind and temperature structure. These parameters were selected because they are likely to be the most variable influence on NBL evolution. A more complete conceptual model of the mesoscale NBL structure was

gained by integrating the results of the numerical simulations with an analysis of the observations.

2. Description of experiments

Since a complete description of the boundary-layer version of the model was given in Part I, only a brief summary of the model's attributes will be given here. It uses a dry quasi-Boussinesq compressible equation set employed in a terrain-following coordinate system. This numerical formulation supports the propagation of both meteorologically significant gravity-wave modes, as well as the acoustic-wave modes using a time-split numerical integration scheme. Turbulent flux terms are evaluated using a K-theory closure in which the eddy exchange coefficients are diagnosed from predicted values of turbulent kinetic energy (TKE) and turbulent length scale (Yamada 1983).

The results from six numerical model experiments are presented for this study. In all of the experiments, the externally imposed winds were not sufficiently strong to prevent the development of the NBL and its associated wind system. Although situations do occur in which very strong synoptic winds overpower the local surface-cooling effects, they are beyond the scope of the present effort, which is focused on the interactions between the NBL winds and the overlying flow. Of the six, one (case 1) was a two-dimensional reference or control case of NBL development similar to the early part of the diurnal simulation that was described in Part I. The model was initialized with an externally imposed westerly wind profile and a deep mixed layer. The mixed layer extended far above the top of a 500-m-high mountain barrier at the eastern end of a long sloping plateau. Two additional two-dimensional simulations (cases 2 and 3) were conducted in which all boundary and initial conditions, except for the imposed external wind speed (U_0 in Table 1) were the same as in the reference case. Two three-dimensional (cases 4 and 5) runs were made in which the external wind profile was the same as that in the reference case, but the direction was altered to provide a component that flowed parallel to the main mountain barrier. A fourth two-dimensional simulation (case 6) was initialized to produce a shallow afternoon mixed layer that was only slightly deeper than the height of the mountain barrier. The results of this experiment are also compared to an observed wintertime case of NBL development. A seventh experiment in which the surface was cooled, but there was no external wind, was also executed as a control case to test the model. A more complete description of the model configuration for these simulations follows.

a. Model domain

Figure 2 shows the domain used in the model simulations. The topography chosen is an idealized representation of an east–west cross section through the study region shown in Fig. 1. A flat plain on the western edge of the domain is bounded on the east by a long sloping plateau with a slope of 0.01. A more steeply sloping ramp with a slope of 0.08 connects the plateau to a 500-m-high blocking ridge on the eastern end of the domain. The mesoscale compensation regions (MCRs) on the lateral boundaries are used for the boundary conditions as described in Part I. The topography for the three-dimensional simulations was a slab-symmetric version of the two-dimensional terrain. For these cases, the interior domain extended 9 km in

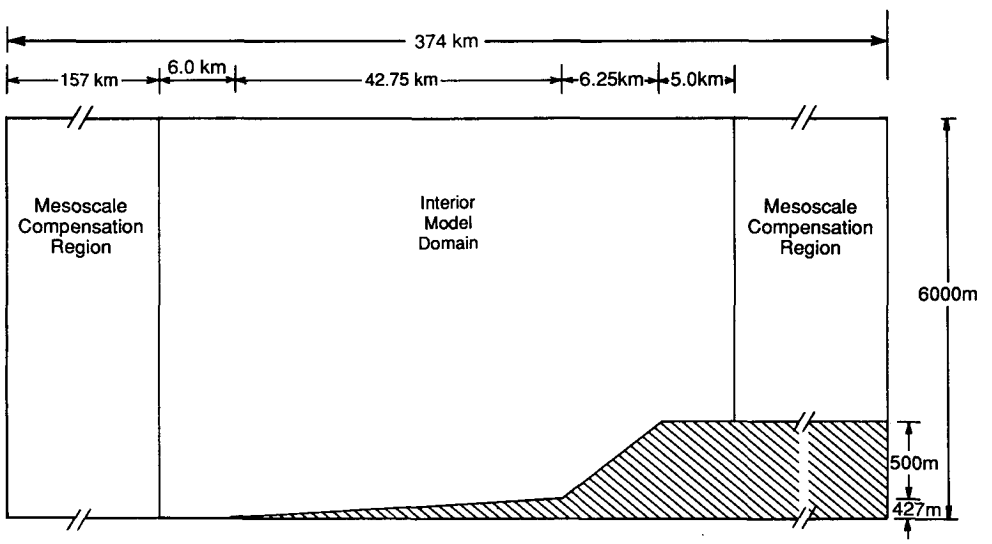

FIG. 2. Model domain (not to scale).

the north–south direction with 31.5-km-wide MCRs between the interior domain boundaries and the north and south external boundaries. Model grid spacing was a constant 375 m in the interior domain for the two-dimensional simulations and was doubled to 750 m for the three-dimensional runs. Vertical grid spacing was a constant 50 m in the lowest 10 layers above the western plain and telescoped logarithmically to include an additional 22 levels below the model top. Vertical spacing above the elevated terrain was proportionally compressed according to the coordinate transformation functions.

b. *Boundary conditions*

The Klemp and Durran (1983) gravity-wave radiation boundary condition was used at the model top. At the model sides, the Orlanski (1976) open lateral boundary condition was coupled with the mesoscale adjustment procedure of Tripoli and Cotton (1982) to inhibit runaway circulations. The externally imposed wind profile is specified at the outer MCR boundaries, and the internal Orlanski boundaries are allowed to adjust to the model mass flow field as the terrain-induced circulations are generated. The surface-layer parameterization was adapted from a formulation by Louis (1979) based on the flux-profile relationships developed by Businger et al. (1971). Surface friction velocity at each point was computed from specified values of the surface roughness and a specified surface kinematic heat-flux function that was derived from field measurements taken in the Brush Creek valley (Doran et al. 1989). This specified flux formulation replaced the crude energy budget described in Part I, which overpredicted the cooling rates in the early part of the simulation. Figure 3 displays the time history of the function that was used to drive the model.

c. *Initialization*

In cases 1–5, the model was initialized with the horizontally homogeneous base-state sounding shown in Fig. 4. A surface-based neutral layer extended from the surface to 1.2 km above the flat western plain. Starting with no wind, the profile shown in Fig. 5 was imposed linearly with time over a 15-min spinup period. The profile was adjusted above elevated terrain to maintain a constant mass flux through the model. Following the initialization, the winds were held fixed at the external MCR boundaries, and a 45-min relaxation period allowed the wind field within the domain to come to steady state. Values for U_0 and V_0 for each of the simulations are shown in Table 1. Surface cooling was initiated after the 1-h period, simulating sunset in the model. Test simulations confirmed that the model had achieved a steady state at this time.

The case 6 initialization was carried out differently from the other five simulations. The stable base-state sounding for this run is also shown in Fig. 4. The wind field was initialized over a 1-h period in the same way

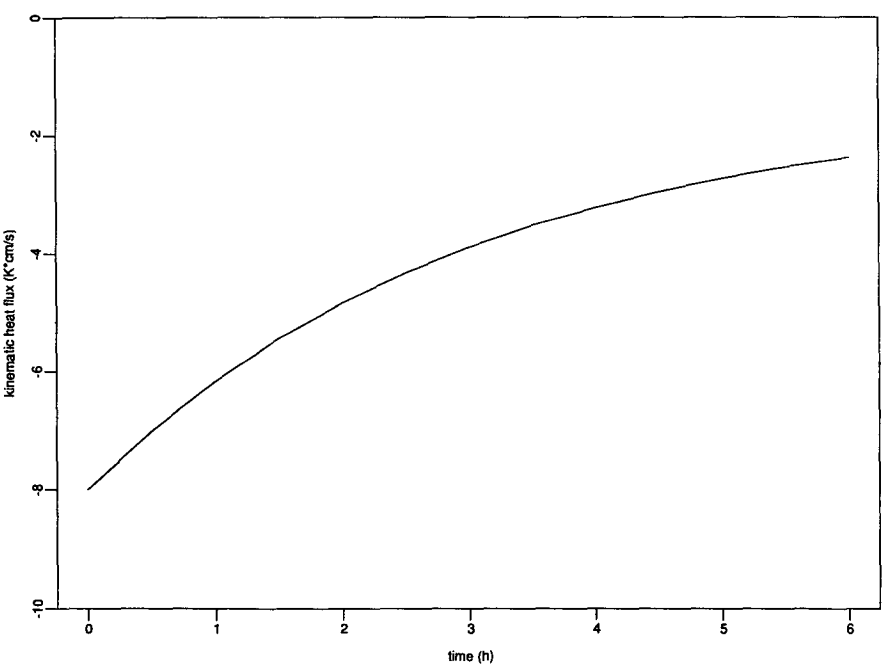

FIG. 3. Sensible heat flux used to drive the model as a function of time after sunset.

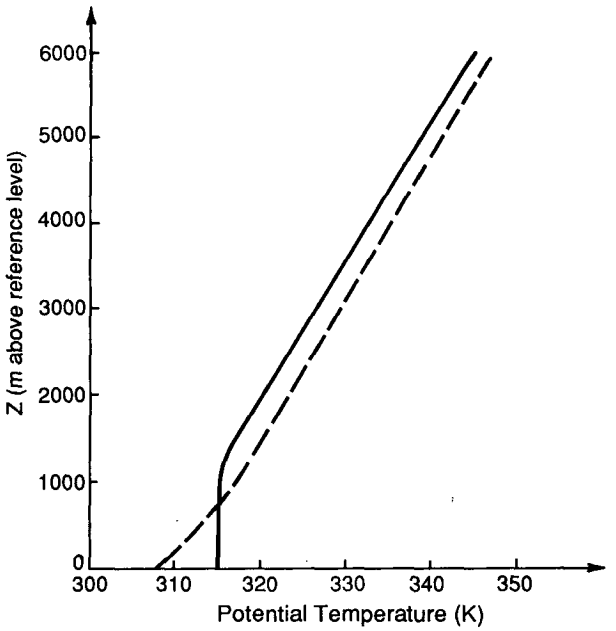

FIG. 4. Model base-state potential temperature profile: cases 1–5—solid line and case 6—dashed line.

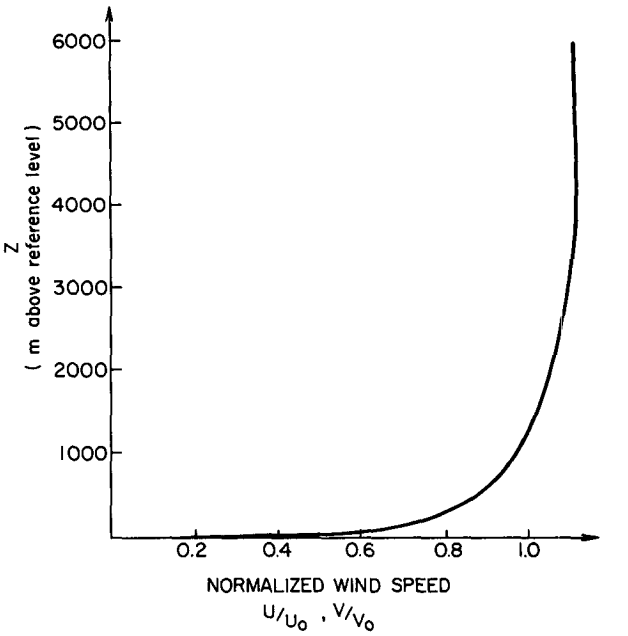

FIG. 5. Externally imposed wind profile. Values of U_0 and V_0 for each simulation are listed in Table 1.

as the other experiments with no surface heat flux. A 4-h heating period followed the dynamic initialization to build a shallow mixed layer typical of that found over snow in the late afternoon. During this period, the surface kinematic heat flux was set to 0.10 K m s^{-1}. Following the 4-h development of a shallow convective layer, the exponentially decaying surface-cooling function shown in Fig. 3 was imposed on the model.

3. Results

Instantaneous fields of all model variables were saved at 10-min intervals for each run. Ten-minute averages of selected variables were computed during the simulations for several vertical grid columns as well. The contour–vector plots in several of the following figures display the instantaneous fields interpolated to a 42 × 42 analysis grid encompassing the lowest 1400 m of the interior model domain. The locations of the vectors in these plots coincide with points on the analysis grid, not actual model grid points. Detailed analysis of the simulation results demonstrated that the interpolation of the model fields did not lead to any misrepresentation of the results.

Figure 6a shows the model wind and potential temperature fields for case 1 at the end of the initialization period. The well-mixed boundary layer is 1300 m deep over the lower terrain and 450 m deep above the blocking ridge to the east. There was virtually no potential temperature gradient in the boundary layer across the domain. After 3 h of cooling (Fig. 6b), the surface inversion had formed, and a weak easterly wind developed in the lowest 75 m above the plateau with speeds ranging from 0.5 m s^{-1} near the base of the ridge to 3.0 m s^{-1} near the plateau–plain junction.

The evening transition was complete 6 h after sunset when a two-layer NBL formed under the remnants of the daytime mixed layer. As can be seen in Fig. 6c, a 75–125-m-deep surface inversion layer is topped by a 100–200-m-deep weakly stable region over most of the sloping plateau. As was described in Part I, the easterly thermal circulations within the surface inversion oppose the prevailing westerly flow, thereby increasing the shear at the top of the inversion layer. The shear promotes the vertical mixing of the cold surface-layer air and forms a weakly stable layer above the surface inversion. As this layer cools, the easterly thermal circulations and the resulting shear-induced vertical mixing gradually extend the NBL deeper into the remnants of the mixed layer through the night. While the surface inversion layer depth is nearly constant along the pla-

TABLE 1. Simulation wind speeds.

Case	U_0	V_0
1	5.0	0.0
2	3.0	0.0
3	7.0	0.0
4	3.5	3.5
5	0.0	5.0
6	0.0	0.0

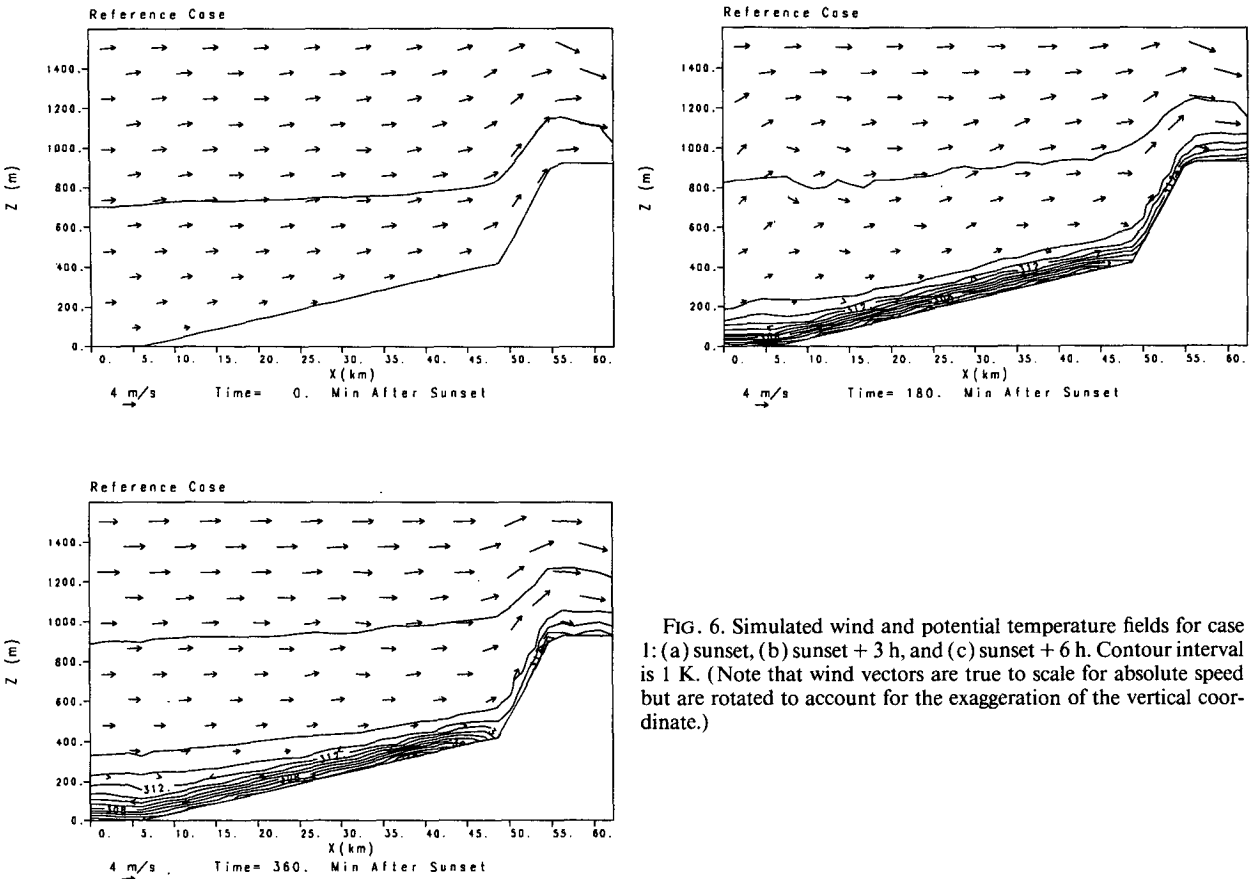

FIG. 6. Simulated wind and potential temperature fields for case 1: (a) sunset, (b) sunset + 3 h, and (c) sunset + 6 h. Contour interval is 1 K. (Note that wind vectors are true to scale for absolute speed but are rotated to account for the exaggeration of the vertical coordinate.)

teau, the transition layer is deeper above the low western plain than it is at the eastern end of the plateau. This is caused in part by the tendency of the cold air in the inversion layer to drain toward lower elevations and pool. Another factor is the dynamic adjustment of the sloping isentropic surfaces through advection and gravity-wave motions. The surface sensible heat flux is sufficiently strong to maintain the inversion layer's slope against these balancing effects, while the turbulent heat-flux divergence in the transition layer cannot cool the transition region rapidly enough to prevent mass adjustment.

Further analysis of the NBL development was performed by examining the evolution of a model "sounding" above a point on the plateau. The temporal development of wind and temperature profiles above a point at $x = 25$ km show the formation of the two-layer structure more clearly. Figure 7a shows that the surface inversion layer cools 3°–7°C in the first hour after sunset and grows slowly after that. This layer is topped by the weakly stable but rapidly growing transition layer that reaches 250–300 m AGL by 6 h after sunset. The thermally driven easterly winds become firmly established with speeds of 2–3 m s^{-1} as the shear layer deepens during the first 4 h after sunset (Fig. 7b). Although the NBL never achieves a steady state, the two-layer structure is completely developed after 5 h, and the NBL growth proceeds more slowly after this time than during the transition period.

a. Effects of wind speed

In cases 2 and 3, the only parameter that was changed from case 1 was the external wind speed U_0. Figure 8 shows the wind and potential temperature profiles for the three runs above $x = 25$ km. Both new simulations exhibit the two-layer structure found in case 1, with stronger external winds forcing the development of a deeper transition layer. Nevertheless, the surface inversion layer exhibits remarkably similar structure in all three cases. The maximum easterly wind speeds vary only from -4.2 m s^{-1} in case 2 to -2.5 m s^{-1} in case 3, despite the difference in U_0 of 4 m s^{-1}. The inversion-layer strength and depth are similar in all three cases as well. However, large differences appear in the structure of the transition layer above the surface inversion. Higher rates of wind shear develop, as would be expected. This shear layer enhances the vertical mixing

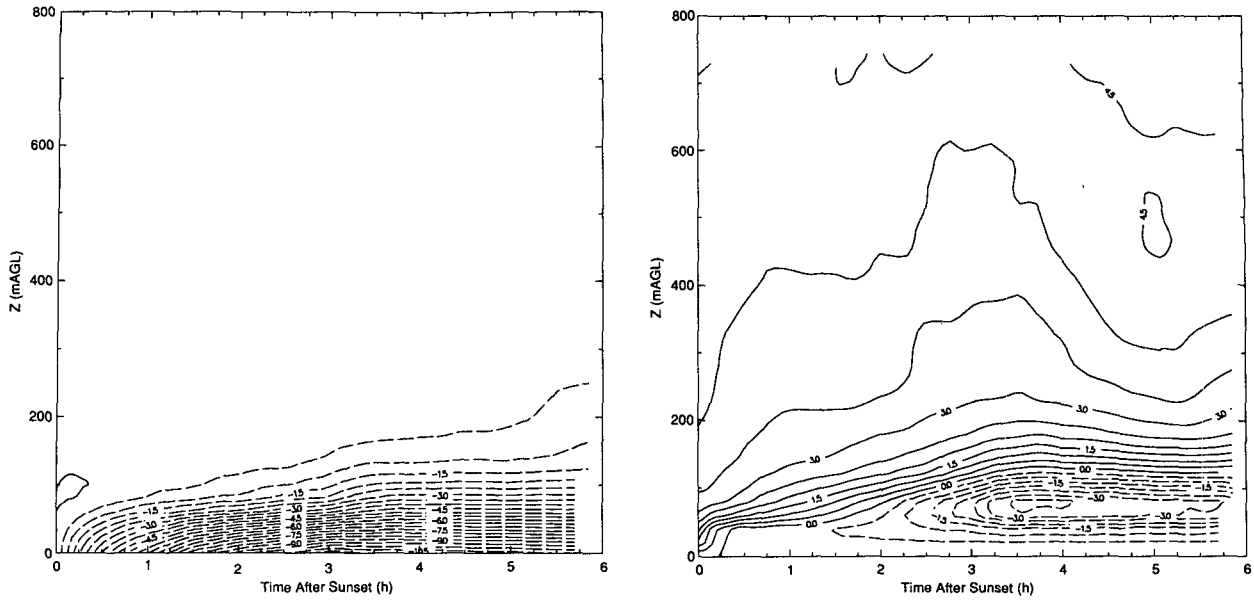

FIG. 7. Evolution of boundary layer above $x = 25$ km for case 1: (a) deviation of potential temperature from the value at sunset and (b) u wind component.

of cold air and contributes to a doubling of the simulated boundary-layer depth from 175 m in case 2 to 350 m in case 3, as defined by the elevation where the stability becomes less than 0.005 K m^{-1}. The total cooling in the column above the point is also greater in the stronger wind case. Since the vertical exchange is enhanced by the stronger shear, more cold air in the surface inversion layer is mixed upward to build the transition layer and less is advected down the slope in the drainage flows.

b. *Effects of wind direction*

The effects of wind direction on NBL evolution were determined by rotating the externally imposed wind profile 45° and 90° to the south in cases 4 and 5, respectively, while keeping the reference wind speed at 5 m s^{-1}. The 6-h structure above $x = 25$ km is plotted for these cases and case 1 in Fig. 9. While the southwest wind case shows little difference in structure from case 1, the south-wind case displays less of a two-layer NBL structure than any of the other cases. A 300–400-m-deep moderately stable layer extended over the length of the plateau with a deeper NBL over the blocking ridge. When the winds are from the southwest U_0 is 3.5 m s^{-1} and the development of the NBL proceeds much like case 2 when U_0 was 3 m s^{-1}. The absence of a wind component into the barrier allows a strong 5–6 m s^{-1} easterly wind to develop that flows down the plateau. This wind is sufficiently strong to drain away much of the colder air near the surface in the latter stages of the simulation when the cooling rate decreases, thereby weakening the stability of the NBL. In the two-dimensional control simulation, in which there was no external wind (both U_0 and V_0 set to 0), a strongly stable, 175-m-deep surface inversion layer formed early in the simulation over the length of the plateau. By 6 h after sunset, however, the stability had weakened dramatically over the eastern half of the plateau as the cold air drained to the western plain and was replaced by warmer air to the east. In contrast to the case 5 simulation, the control experiment did not simulate the formation of the deep, weakly stable NBL. The absence of the directional wind shear at the top of the inversion layer prevented the cold inversion-layer air from mixing upward.

c. *Effects of initial mixed-layer depth*

The most significant differences between the summer and winter structure of the mesoscale boundary layer result from the large differences in daytime surface sensible heat flux between the two seasons. This is particularly true when snow cover over the region reduces the daytime mixed-layer growth. In Part I, data were presented from two summertime cases of NBL structure when the sunset mixed-layer depth greatly exceeded the elevation of the highest terrain in the region. For contrast, wintertime observations were made of NBL development over the Roan Plateau from 0000 to 0060 UTC (1600–2200 LST) 21 January 1984. During this period, the study region was on the anti-

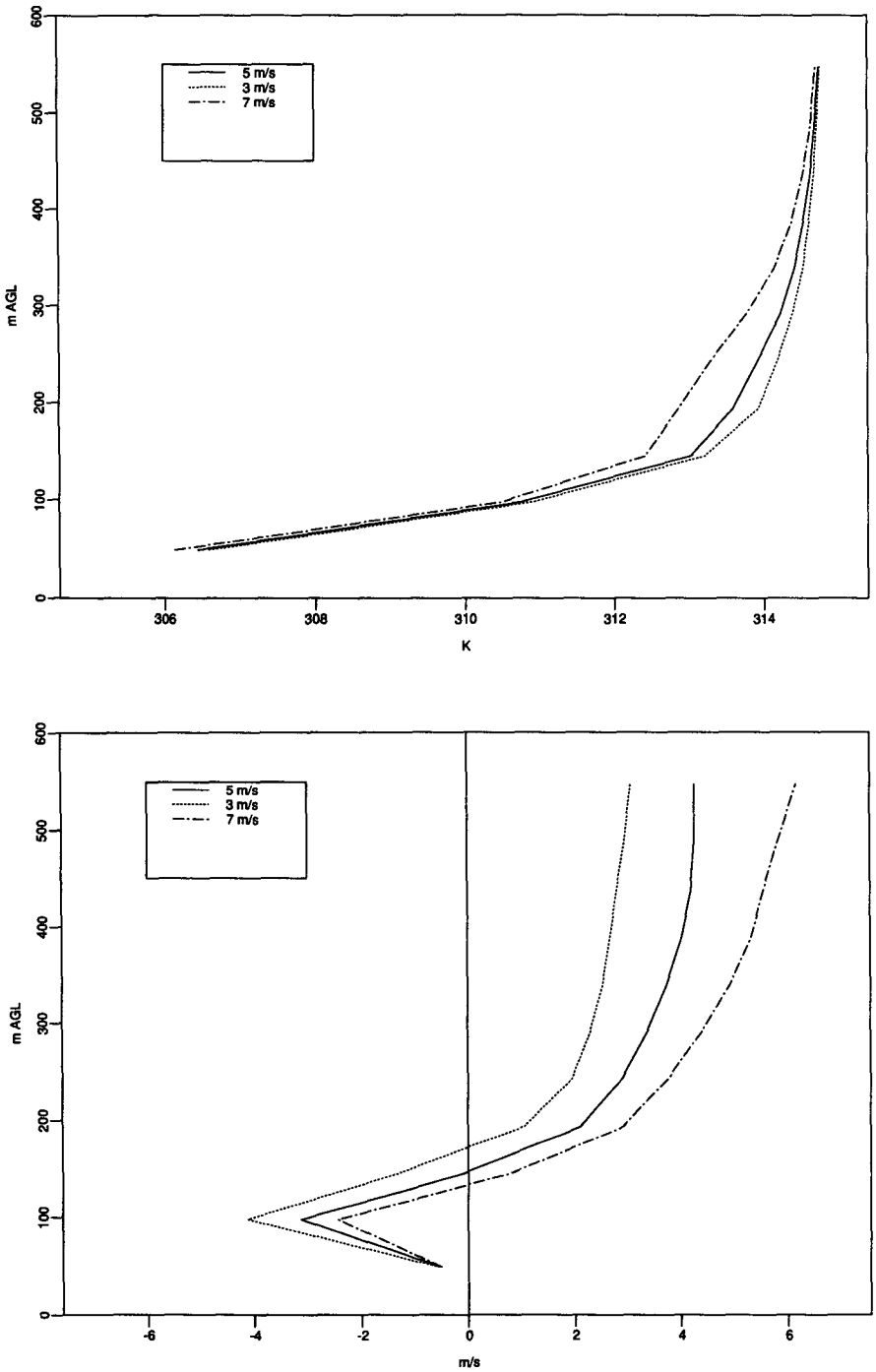

FIG. 8. Sunset + 6 h profiles above $x = 25$ km for cases 1–3: (a) potential temperature and (b) u wind component.

cyclonic side of the primary polar jet axis following the passage of a major storm five days earlier. Temperatures remained cold in the intervening period so that 23 cm of snow remained on the ground at Grand Junction, and snow covered much of the area. Winds were from the northwest at 15.0 m s^{-1} at 4000 m MSL in the 0000 UTC (1700 LST) Grand Junction National Weather Service sounding. This pattern remained sta-

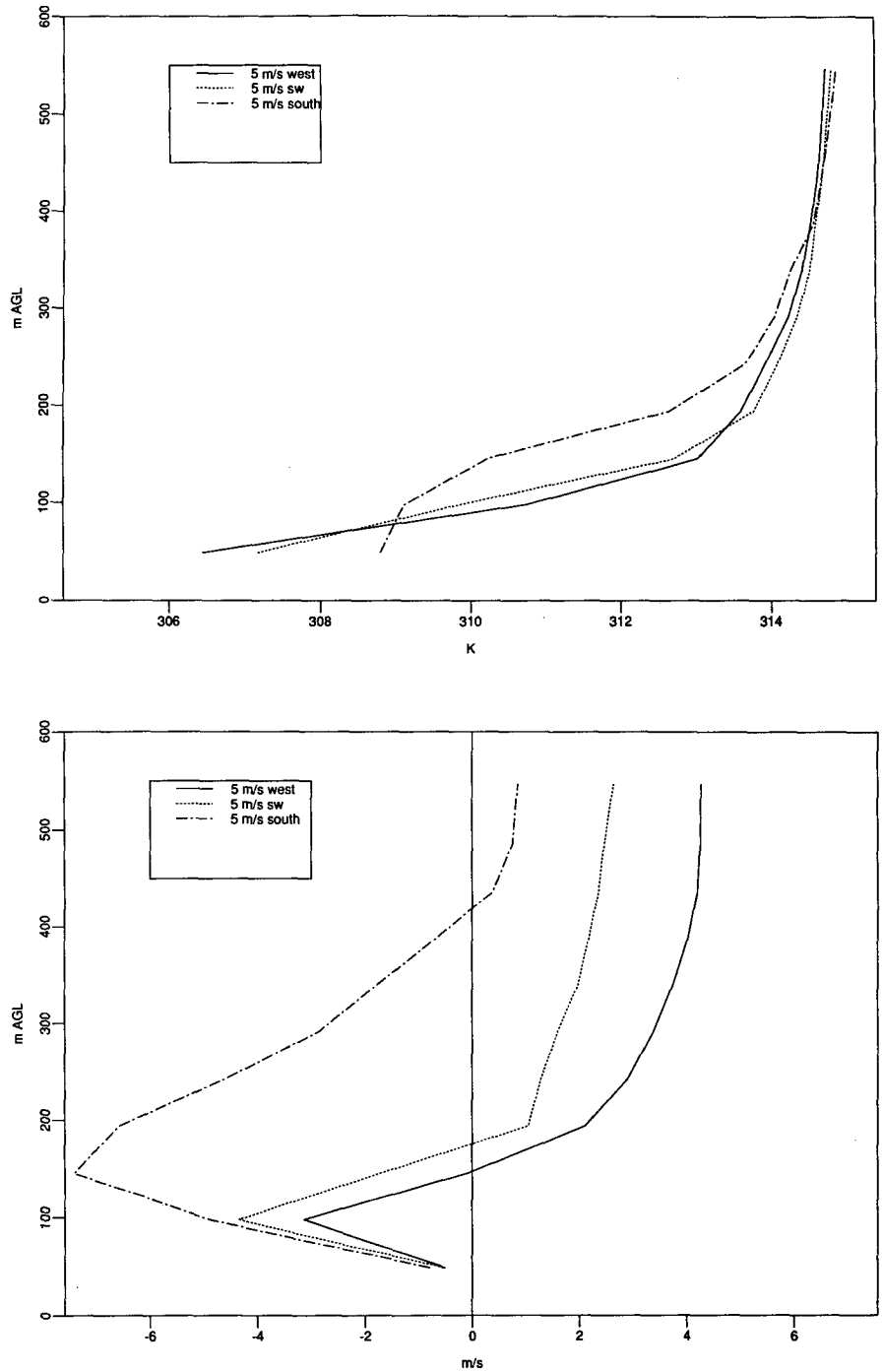

FIG. 9. Same as 8 but for cases 1, 4, and 5.

ble through most of the evening, and the skies were clear. The primary data used to analyze NBL evolution were vertical soundings of wind and temperature taken every 2 h from the Ca and Rifle sites shown in Fig. 1. The Rifle site was in the Colorado River valley on the southeast side of the plateau, while the Ca site was located on the plateau's northwest slope. Gradient-level winds approximately traversed a transect between the two sites.

Figure 10 shows the 1600 LST sounding from the Ca site. Above the shallow surface inversion was a 500-m-deep mixed layer that extended above the Roan

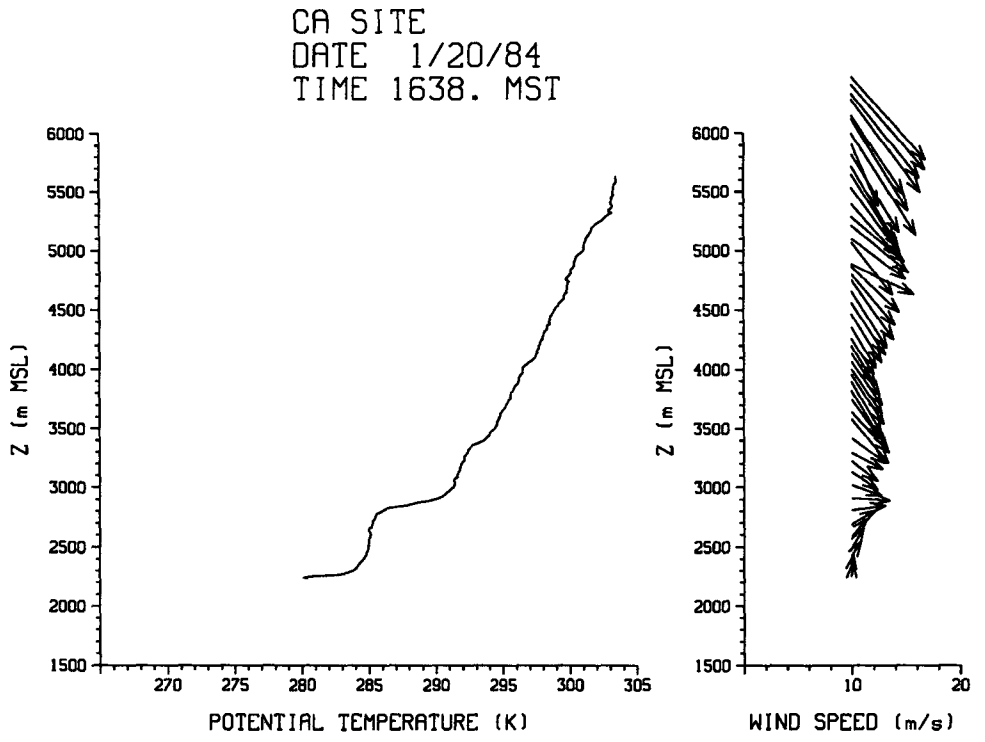

FIG. 10. 1600 LST sounding from Ca site.

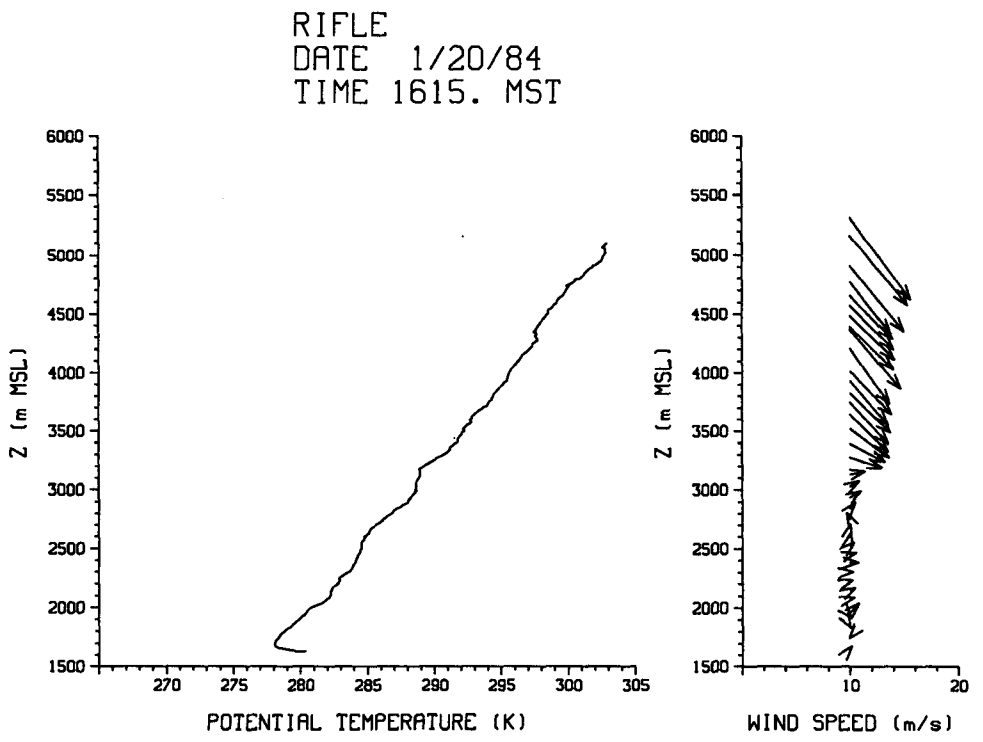

FIG. 11. 1600 LST sounding from Rifle site.

Plateau (elevation, 2500–2600 m MSL). The south winds in the lower layers turn northwesterly with height. At Rifle, the boundary layer was already stably stratified through its depth by the time the first sounding was made (Fig. 11). By launch time, the river valley was in shade, and surface cooling had probably begun over the area. The strong shear layer at 3200 m MSL indicated the dividing streamline that separated the lower blocked layers from the air that flows over the high topography to the southeast.

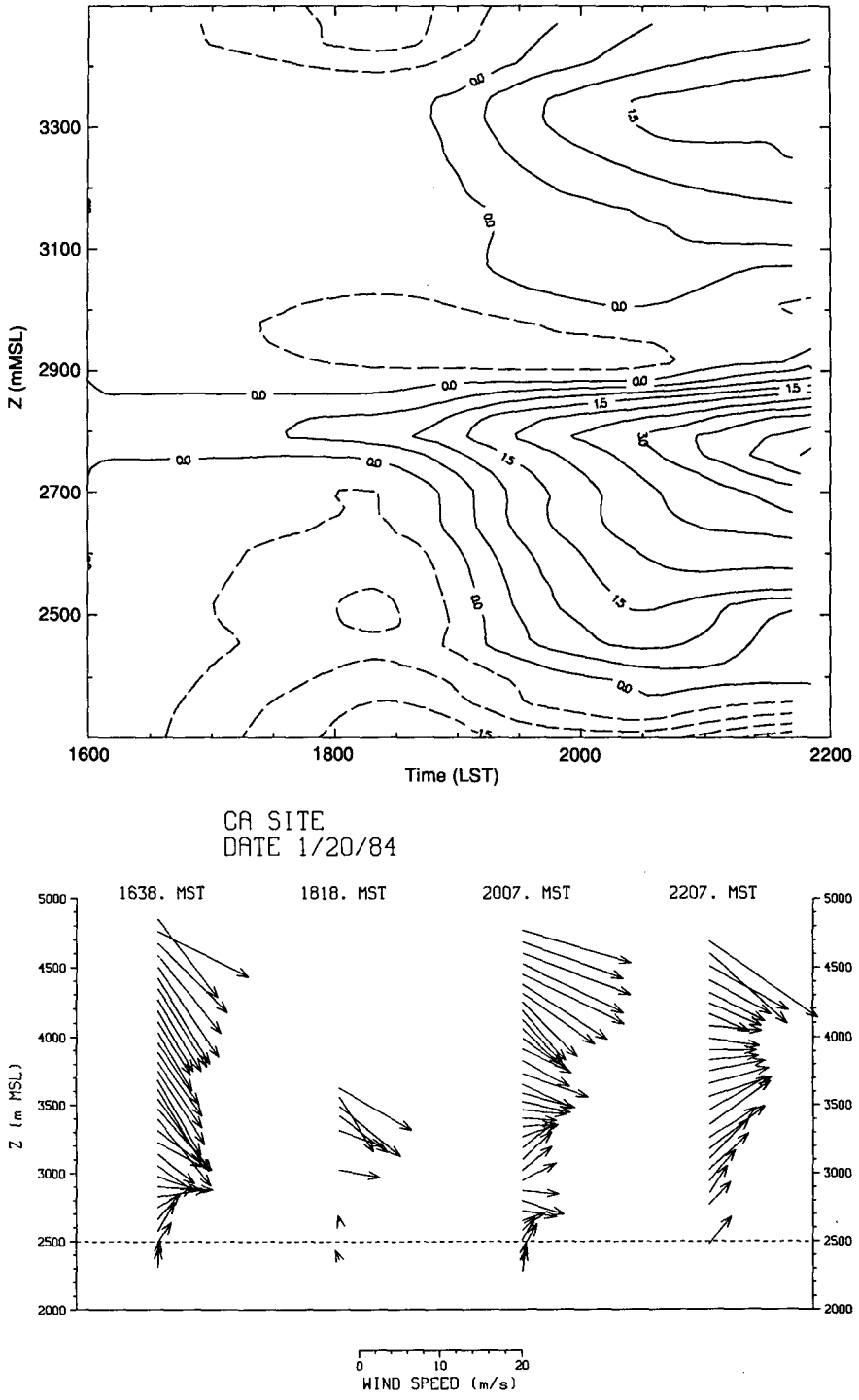

FIG. 12. Evolution of the NBL above Ca: (a) deviation of the potential temperature from 1600 LST sounding and (b) wind profile.

Figure 12 displays the development of the NBL structure as deduced from the series of soundings made at the Ca site. Following the early cooling, synoptic-scale warm advection produced a 1–2-K increase above 2400 m MSL. Additionally, there was little influence of the mesoscale NBL on the evolution of the wind profile. The observed veering of the wind with height in the later soundings was a by-product of the warm advection. In contrast to the Ca data, the Rifle NBL evolution was heavily influenced by the high terrain of

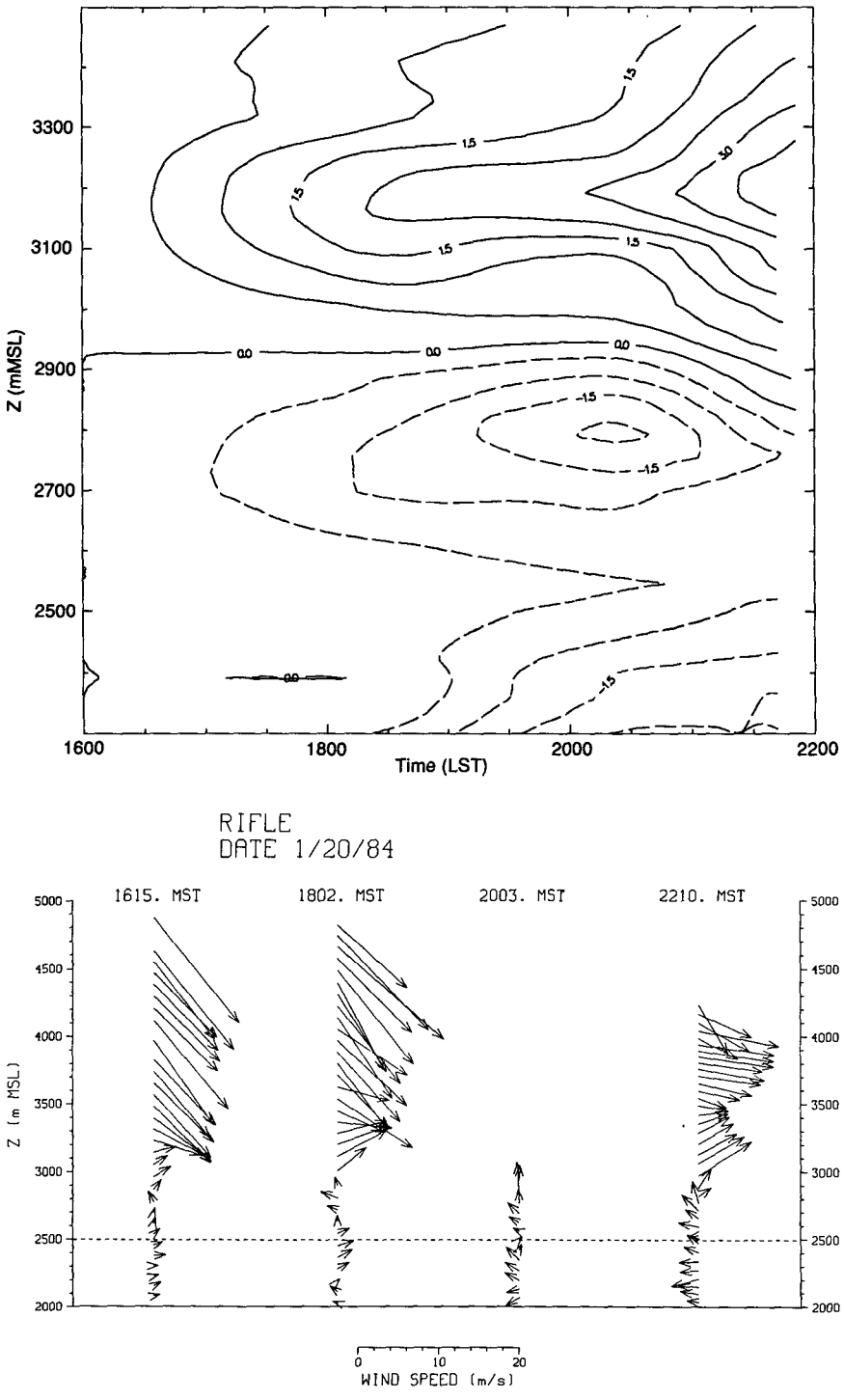

FIG. 13. Same as Fig. 12 but for Rifle.

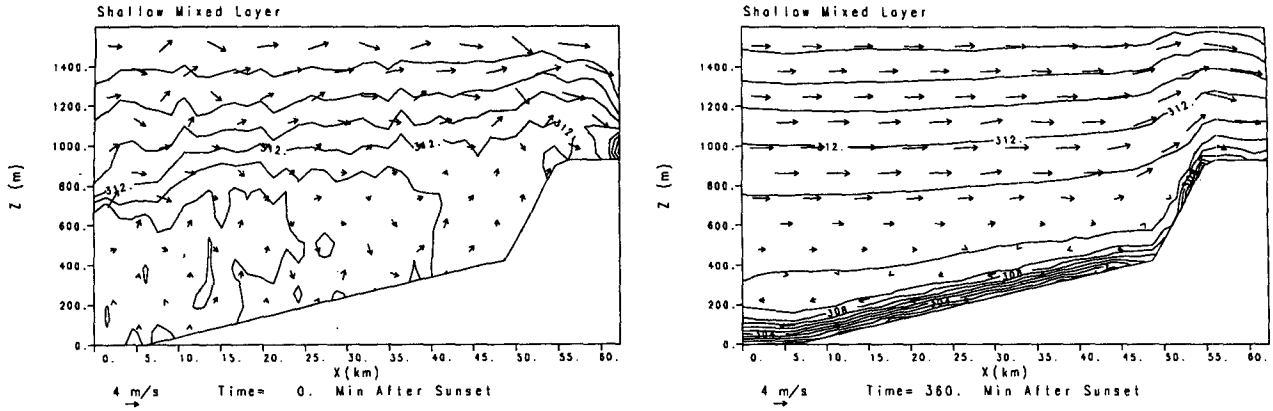

FIG. 14. Simulated wind and potential temperature fields for case 6: (a) sunset and (b) sunset + 6 h. Contour interval is 1 K.

the Roan Plateau to the northwest and high mesas to the southeast (Fig. 13). The thermally forced flow below 2900 m MSL coincided with a cooling region under a deeper warming layer. The southeast winds grew stronger as the evening progressed, reaching 2–3 m s^{-1} by 2200 LST. At higher levels, the winds shifted sharply to a 6–7 m s^{-1} southwesterly flow at 3000 m MSL, which was consistent with the winds observed at Ca. The dividing streamline descended 200–300 m since the first sounding at 1600 LST, despite the upper-level warm advection that would tend to increase the stability in the layer.

Case 6 simulated the development of the NBL when the afternoon mixed layer is shallow, as was found during the winter when high surface albedos caused by snow and low solar zenith angles combined to reduce the daytime sensible heating. Figure 14a shows the sunset state of the model boundary layer at the conclusion of the initialization period. A 600–700-m-deep convective layer developed under a quasi-isothermal layer that extended to the 1400-m elevation above the low western plain. The winds within the mixed layer were not strong enough to flow over the barrier, producing a blocked flow region on the upwind side. Six hours later (Fig. 14b), the mixed layer has been replaced by a two-layer NBL. Overlying the surface-layer easterly winds is a free-flowing 1.0–6.0 m s^{-1} westerly wind through the region where the flow was previously blocked. A combination of reduced turbulent drag near the surface and the cooling of the layer above the ridge eliminated the energy difference between the air above the plateau and that over the ridge. This result is con-

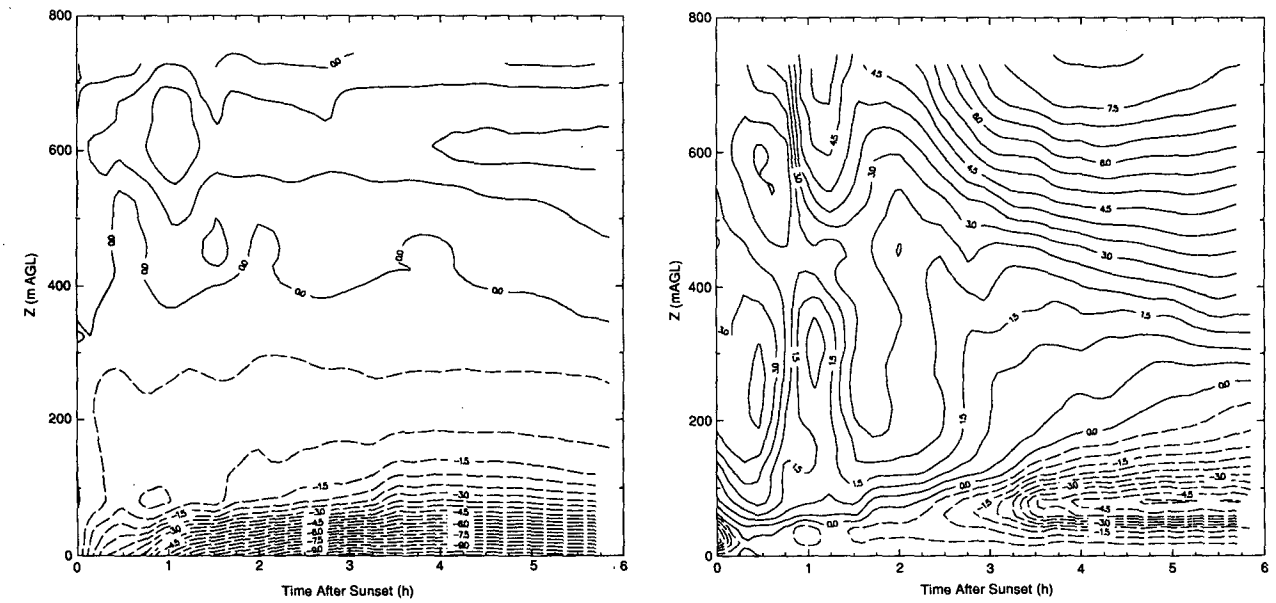

FIG. 15. Evolution of boundary layer above x = 25 km for case 6: (a) deviation of potential temperature from the value at sunset and (b) u wind component.

sistent with the Rifle observations, which show a similar shrinking of the blocked flow region as the NBL developed. The evolution of the NBL above $x = 25$ km is shown in Fig. 15. Like the other cases, a 100–150-m-deep surface inversion layer develops above the plateau with 3–4 m s^{-1} easterly winds. The transition layer merges with the overlying isothermal region to form a deep stable layer. Higher-level winds increase in speed during the first 2 h after sunset to 6–7 m s^{-1}.

4. Analysis of results

Except for the case when there was no component of the prevailing wind into the barrier, the development of a two-layer NBL was simulated in all of the model simulations. The strong surface inversion present in the simulations would not be uniformly observed over the Roan Plateau, since the surfaces are very irregular and contain many depressions and valleys. Neverthe-

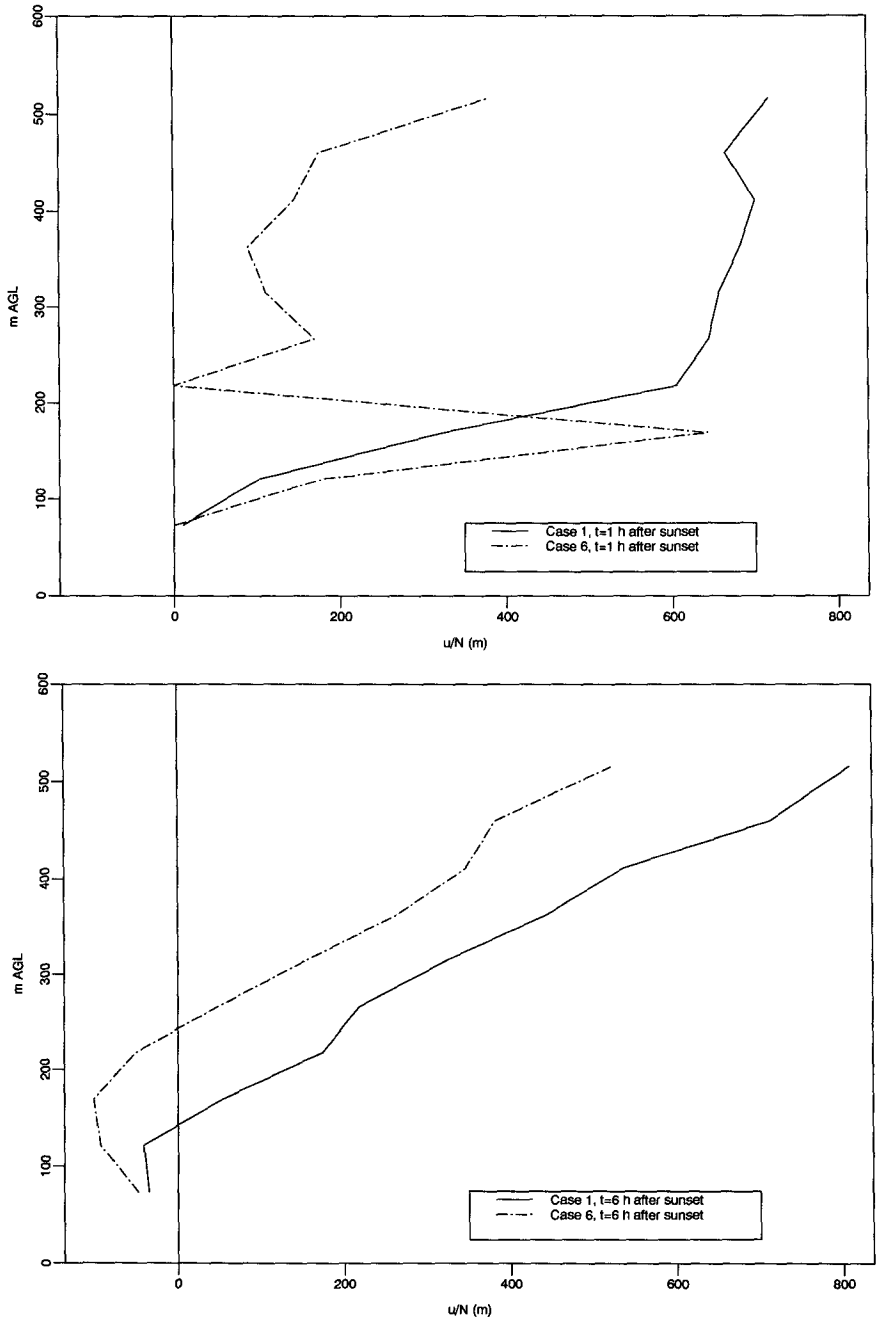

FIG. 16. Profiles of uN^{-1} above $x = 25$ km for cases 1 and 6: (a) 1 h after sunset and (b) 6 h after sunset.

less, this two-layer structure is consistent with the observations shown in both Part I and the current paper. In all cases, the NBL grows deeper than those observed over flat terrain, a consequence of the increased shear produced by the development of terrain-induced thermal circulations. The primary effect of more than doubling the wind speed was to double the depth of the transition layer. Like NBL structure over flat terrain, to a first approximation the transition-layer depth is proportional to the wind speed (Zilintinkevich 1972). However, this deep layer developed differently in the absence of a component into the barrier, as was simulated in case 5. Directional wind shear between the thermal circulations and large-scale flow was sufficient to build the deep NBL. The most interesting result of this study was the lack of significant differences between the summertime and wintertime simulations. Afternoon boundary-layer depth did not have a strong influence on the resultant quasi-steady nocturnal structure. Figures 16a and 16b show profiles of the value uN^{-1} (N is the Brunt–Väisällä frequency) 1 and 6 h after sunset for cases 1 and 6. This parameter is used in potential-flow theory to compute the dividing-streamline height for stratified flow over a barrier. Briefly, it is the change in elevation a parcel can achieve if its kinetic energy is converted entirely to potential energy, assuming constant stability of the layer. The negative values in Fig. 16b are meaningless in this context, as they result from the low-level thermal circulation. The two different afternoon flow regimes evolved to a very similar structure within 6 h, which can be interpreted as a boundary-layer time scale for the combined mechanical–thermal circulation. This time scale is much shorter than the inertial time scale of approximately 17 h, implying that Coriolis effects, although significant, are secondary to the thermal and mechanical effects of the terrain. Additionally, the differences in the NBL development between the Ca and Rifle sites show that the mesoscale NBL is limited in extent and is influenced greatly by the mesoscale landforms in the region.

5. Conclusions

Several factors influencing mesoscale development of the NBL above a large sloping plateau upwind of a high mountain barrier were simulated using a dynamical model. The results show that a 3–4 m s^{-1} thermal topographic circulation develops in a 100–200-m inversion layer, despite the strength of the opposing large-scale winds. The NBL consists of a two-layer structure with a strongly stable, shallow, surface inversion layer capped by a 200–500-m-deep, less stable transition layer. This complicated layer structure makes routine Froude-number calculations to determine dividing-streamline height impractical in these instances. The two-layer structure appears in cases when the daytime mixed-layer depth is greater than the blocking-ridge height as well as when the mixed layer is shallow and the flow is blocked. The persistence of thermally generated valley and slope winds in all seasons and through a wide range of large-scale meteorological conditions is a result of the buffering effect of the mesoscale NBL coupled with the mechanical topographic sheltering.

Acknowledgments. This research was supported by the U.S. Department of Energy (DOE) under Contract DE-AC06-76RLO 1830. Computer model simulations were run on the computers at the National Energy Research Supercomputer Center. Pacific Northwest Laboratory is operated for DOE by Battelle Memorial Institute. Preliminary studies were funded by the National Science Foundation (NSF) under Grant ATM83-04328, and early computer simulations were run at the National Center for Atmospheric Research, which is sponsored by NSF.

REFERENCES

Bader, D. C., T. B. McKee, and G. J. Tripoli, 1987: Mesoscale boundary layer evolution over complex terrain. Part I: Numerical simulation of the diurnal cycle. *J. Atmos. Sci.*, **44,** 2823–2838.

Businger, J. A., J. D. Wyngaard, Y. Izumi, and E. F. Bradley, 1971: Flux profile relationships in the atmospheric surface layer. *J. Atmos. Sci.*, **28,** 181–189.

Doran, J. C., M. L. Wesely, R. T. McMillan, and W. D. Neff, 1989: Measurements of turbulent heat and momentum fluxes in a mountain valley. *J. Appl. Meteor.*, **28,** 438–444.

Klemp, J. B., and D. R. Durran, 1983: An upper boundary condition permitting internal gravity wave radiation in numerical mesoscale models. *Mon. Wea. Rev.*, **111,** 430–444.

Louis, J., 1979: A parametric model of vertical eddy fluxes in the atmosphere. *Bound.-Layer. Meteor.*, **17,** 187–202.

Orlanski, I., 1976: A simple boundary condition for unbounded hyperbolic flows. *J. Comput. Physics,* **21,** 251–269.

Tripoli, G. J., and W. R. Cotton, 1982: The Colorado State University three-dimensional cloud/mesoscale model-1981. Part I: General theoretical framework and sensitivity experiments. *J. Rech. Atmos.*, **16,** 185–219.

——, and ——, 1986: An intense, quasi-steady thunderstorm over mountainous terrain. Part IV: Three-dimensional numerical simulation. *J. Atmos. Sci.*, **43,** 894–912.

Yamada, T., 1983: Simulations of nocturnal drainage flows by a q^2–l turbulence closure model. *J. Atmos. Sci.*, **40,** 91–106.

Zilintinkevich, S. S., 1972: On the determination of the height of the Ekman boundary layer. *Bound.-Layer Meteor.*, **3,** 141–145.